Ultrasonics - Sonochemistry 44 (2018) 184–195

Contents lists available at ScienceDirect

Ultrasonics - Sonochemistry

journal homepage: www.elsevier.com/locate/ultson

Rod-shaped cavitation bubble structure in ultrasonic field

Bai Lixin[a,*], Wu Pengfei[a,b], Liu Huiyu[c,*], Yan Jiuchun[d,*], Su Chang[a], Li Chao[a]

[a] State Key Laboratory of Acoustics, Institute of Acoustics, Chinese Academy of Sciences, Beijing 100190, China
[b] University of Chinese Academy of Sciences, Beijing 100049, China
[c] Beijing Key Laboratory of Bioprocess, Bionanomaterials & Translational Engineering Laboratory, Beijing University of Chemical Technology, Beijing 100029, China
[d] State Key Laboratory of Advanced Welding and Joining, Harbin Institute of Technology, Harbin 150001, China

ARTICLE INFO

Keywords:
Ultrasonic cavitation
Cavitation structure
Rod-shaped structure
Y-branch structure
Smoker structure

ABSTRACT

Rod-shaped cavitation bubble structure in thin liquid layers in ultrasonic field is investigated experimentally. It is found that cavitation structure successively experiences several stages with the change of the thickness of the thin liquid layer. Rod-shaped structure is a stable structure of the boundary between the cavitation cloud region and the non-cavitation liquid region, which can be formed in two different ways. Cavitation bubbles in a thin liquid layer have a distribution in the thickness direction. The rod-shaped structures tend to crosslink with each other to form stable Y-branch structures. The angle of the Y-branch structure is Gauss distribution with mathematical expectation $\mu = 119.93$. A special rod-shaped cavitation structure with source is also investigated in detail. Due to the pressure gradient in the normal direction, the primary Bjerknes force causes the bubbles in the rod-shaped structure on both sides to converge to the axis. The secondary Bjerknes forces between the bubbles also make the cluster converge, so the large bubbles which are attached to the radiating surface tend to align themselves along the central line. According to the formula deduced in this paper, the variation of curvature of curved rod-shaped structure is qualitatively analyzed. The Y-branch structure of cavitation cloud and Plateau boundary of soap bubbles are compared.

1. Introduction

Cavitation refers to the formation and subsequent dynamic life of bubbles in liquids subjected to a sufficiently low pressure. Applications of cavitation span many industrial sectors, from ultrasonic brazing, through ultrasonic lithotripsy, sonochemistry, ultrasonic cleaning, and wastewater treatment, to jet cutting [1]. The mechanical and chemical effects of cavitation are responsible for these applications. Each bubble in the cavitation field acts as a single shock wave generator or a sonochemical reactor. The visual observations indicate that cavitation bubbles rarely exist in isolation and are present in the form of clusters or clouds. However, the spatial distribution of these bubbles is normally not homogeneous, forming different structures in the ultrasound field [2]. Moussatov et al. [3] found that the macro-structure of the CBS in the vicinity of the radiating surface remains remarkably stable, though the streamers in the structure are not stable and fluctuate in space. Dubus et al. [4] explained the physical origin of conical bubble structure under an ultrasonic horn by a hypothesis of nonlinear thickness resonance. He also highlighted the role of geometrical focus of bubble structures. Louisnard et al. [5] found that the conical structure is generic and results from the appearance a sound velocity gradient along the transducer area, and strong energy dissipation by inertial bubbles is a key mechanism ruling the structure of the acoustic field in a cavitating medium. Bai et al. [6] investigated conical bubble structures in the vicinity of the radiating surface by high-speed photography. He found that different vibration modes result differences in the direction of acoustic radiation forces, and the disparity of the direction of acoustic radiation forces lead to differences in the structure of conical bubble structure. Akhatov et al. [7] developed a model for the theoretical description of one- and tow-dimensional structure formation in bubble–liquid mixtures. Parlitz et al. [8] (1999) and Mettin et al. [9] (1999) reproduced acoustic Lichtenberg figure structures in simulations by the assumption of an inhomogeneous distribution of bubble sources in space. Bai et al. [10,11] investigated experimentally smoker cavitation structure and the cavitation structures produced by artificially implanting nuclei. They formed bubble letters in the tailing zone by controlling the nuclei. Mettin et al. [12] and Krefting et al. [13] investigated jellyfish bubble structures in an ultrasonic standing wave field at 40 kHz by high-speed photography.

The conditions and characteristics of different types of cavitation structures are different. The cavitation in a thin liquid layer was first investigated by Moussatov et al. [14]. They found that this

* Corresponding authors.
E-mail addresses: blx@mail.ioa.ac.cn (L. Bai), liuhy@mail.buct.edu.cn (H. Liu), jcyan@hit.edu.cn (J. Yan).

https://doi.org/10.1016/j.ultsonch.2018.02.030
Received 2 November 2017; Received in revised form 26 January 2018; Accepted 15 February 2018
Available online 16 February 2018
1350-4177/

configuration leads to a large amplification of the acoustic pressure which makes the generation of cavitation possible at low power or in a wide frequency range. García-Atance Fatjó et al. [15] investigated the cavitation ring in a thin liquid layer using a theoretical model based on the combination of Fluid Mechanics and Analytical Mechanics. Bai et al. [16,17] and Wu et al. [18] investigated the memory effect, surface tension and the macro stability of cavitation bubble cloud in a thin liquid layer by high-speed photography. A long-term (several-second duration) memory effect was discovered in the thin liquid layer. The existence of surface tension on the interface of liquid region and cloud region is proved in their study. A competition and dynamic balance of two processes with a negative feedback mechanism was proposed to explain the stability of cavitation structures and their transformation.

In this paper, rod-shaped cavitation bubble structure in a thin liquid layer is investigated. Fernandez Rivas [19] and Zijlstra [20] produced, but did not study the strip-shaped bubble structures on a silicon surface (these bubbles are artificially nucleated by microfabricated small pits on a silicon chip), which is very similar to the rod-shaped cavitation bubble structure in a thin liquid layer. The present work is, from the authors' knowledge, the first analysis of rod-shaped or strip-shaped cavitation structures in an acoustic field.

2. Experiment

The experimental diagram is shown in Fig. 1. The ultrasonic horn is mounted horizontally in a transparent chamber (600 mm × 330 mm × 330 mm). A glass plate (thickness, $b = 5$ mm) is used as reflector which can be moved back and forth horizontally by controlling the stepper motor (minimum adjustment distance: 20 μm). The piezoceramic sandwich transducers are enveloped in a shell and can be submerged in water completely. The high power ultrasound is produced by three ultrasonic processors (Jiuzhou Ultrasonic Technology Co., Ltd. China) with a frequency of 20 kHz (radiating surface diameter, $d = 50$ mm), 30 kHz ($d = 38$ mm) and 40 kHz ($d = 30$ mm) and a maximum input electric power of 100 W. Cavitation structure in the thin liquid layer (front view and side view) is recorded by a high-speed camera (Photron Fastcam SA-1, Photron Ltd., Japan) equipped with two long distance microscopes (Zoom 6000, Navitar, USA; LM50JCM, Kowa, Japan) respectively. The frames are illuminated with a PI-LUMINOR high-light LED lamp (150 W) and a HYLOW xenon flash lamp (duration time: 4 ms). Fresh tap water (with many nuclei) is used in the experiment so as to reduce the cavitation threshold. The similar results can be obtained in deionized water but with few cavitation bubbles, as compared to in tap water.

3. Results and discussion

3.1. Feature element of cavitation structures in thin liquid layers

Some typical results for different frequency and different liquid layer thickness are shown in Fig. 2. It can be seen that cavitation structure successively experiences several stages such as spotted structure (as shown in Fig. 2(A1) and (C1)), disc-shaped structure (as shown in Fig. 2(A3–A6), (B2–B4) and (C2–C4)), rod-shaped structure (as shown in Fig. 2(A7–A9), (B4–B5) and (C4–C5)), and smoker structure (as shown in Fig. 2(A10), (B6) and (C6)). It is found in experiments that power has a greater influence on cavitation structures than frequency and radiation surface area. In the same liquid layer thickness, the morphology of cavitation cloud will evolve to a forward form (a cavitation structure in thinner layer thickness) with the increase of power. When the amplitude of radiation surface is large enough, the cavitation structures in thin liquid layers that mentioned in Fig. 2 will appear on the radiating surface of the transducer without reflection plate on the opposite side. Smoker structure and rod-shaped structure have been found on the radiating surface without reflection, and it is speculated that as the power increases, other cavitation structures will also be found. The influence of power on the cavitation structure is very large. The influence of the thickness of a thin liquid layer on the cavitation structure is not unique. Therefore, the absolute value of the thin layer thickness is not particularly important. However, with the change of the thickness of the thin liquid layer, the morphology and occurrence order of cavitation structures are deterministic. Take 20 kHz as an example to classify the cavitation structure, and 30 kHz and 40 kHz experienced a similar process.

3.1.1. Spotted structure ($h < 100\,\mu m$)

When the radiating surface of the transducer is very close to the reflecting surface (glass plate), the reflecting surface is subjected to strong radiation force (near-field acoustic levitation), so that the two surfaces are difficult to fit completely. When we apply sufficient force to

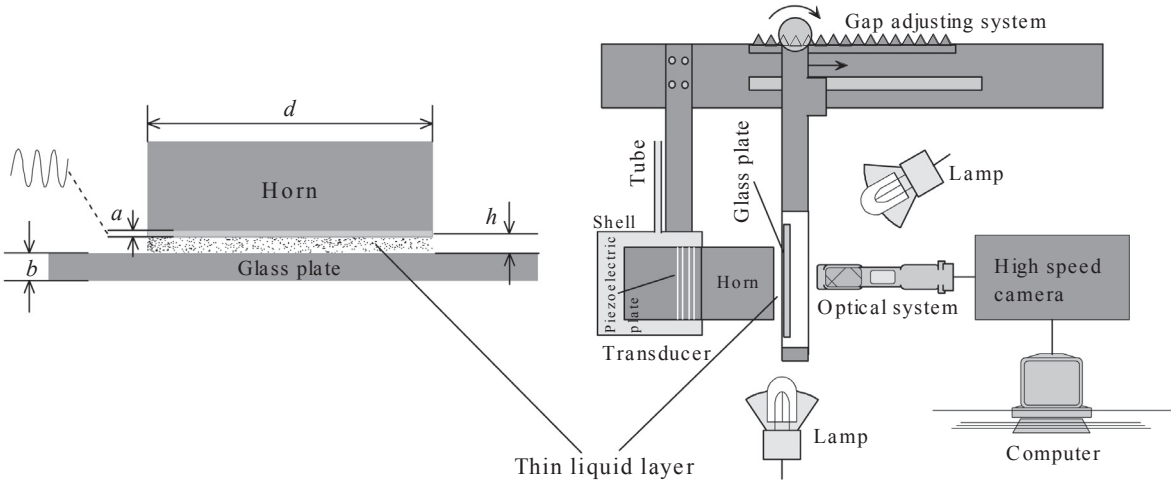

Fig. 1. Experimental set-up to visualize the rod-shaped cavitation structure in a thin liquid layer of varying thickness. Step motor-driven gap adjusting system is used to fix the transducer and adjust the distance (liquid layer thickness, h) between the radiating surface and glass plate (reflector). The left schematic diagram depicts the geometric parameters used in this study (see text).

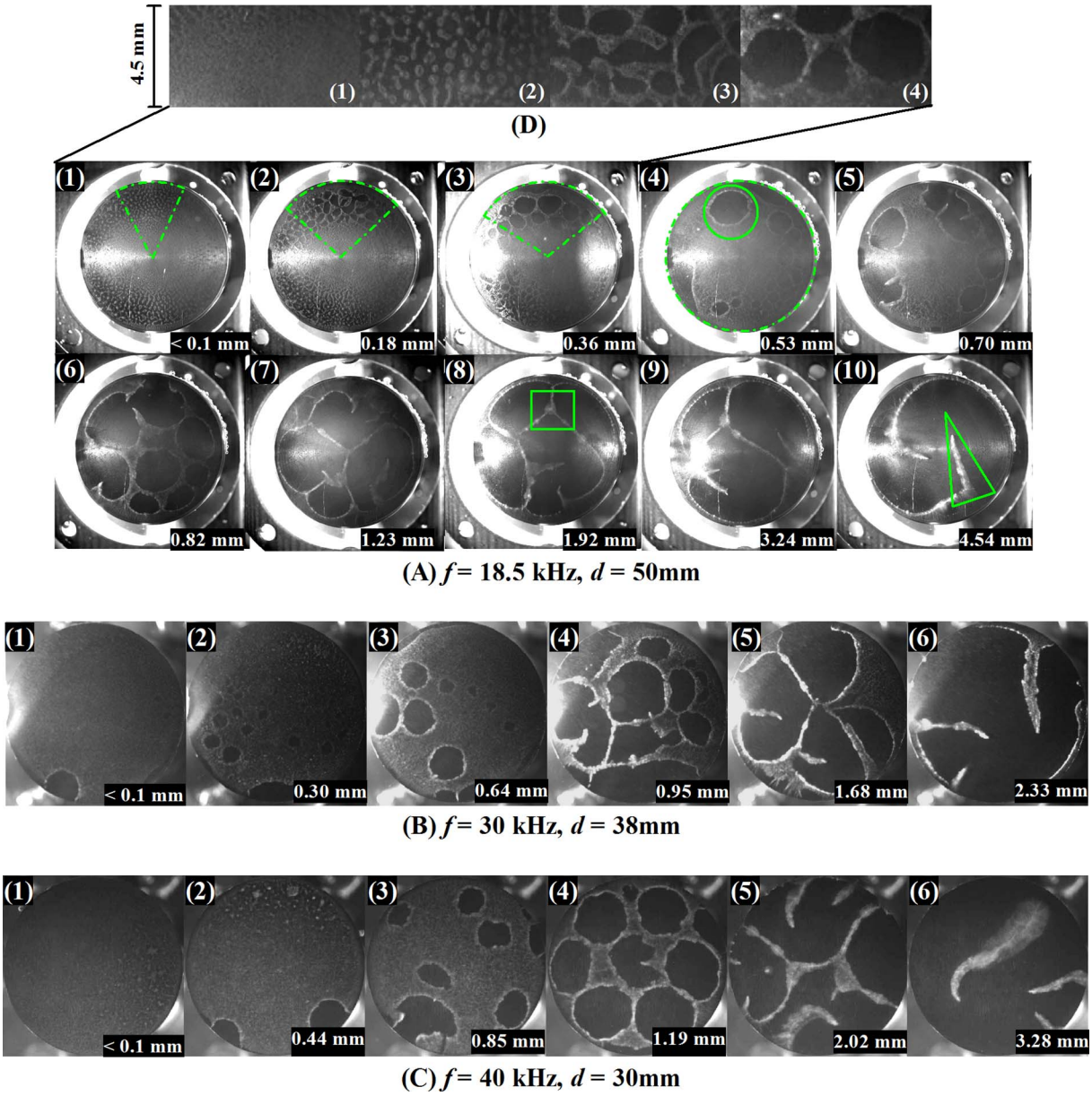

Fig. 2. Cavitation structures as a function of liquid layer thickness (h). The liquid layer thickness is shown on the bottom right corner of each frame. Light areas are cavitation region (cavitation bubble cluster), and dark areas are non-cavitation region (water without bubbles). (A) Frequency is 18.5 kHz, diameter of radiating surface is 50 mm. The upper inset depicts the details of cavitation clusters (h < 0.36 mm); (B) Frequency is 30 kHz, diameter of radiating surface is 38 mm; (C) Frequency is 40 kHz, diameter of radiating surface is 30 mm.

make h < 100 μm, the cavitation cloud in the center of the thin liquid layer is uniformly distributed, and the cavitation cloud in the periphery of the thin liquid layer shows a spotted distribution (as shown the upper inset depicts the details of cavitation clusters in Fig. 2(A)). The spotted cavitation bubble cluster is round-shape (diameter: 0.5 mm). The continued increase in preload force seems to have no effect on cavitation structure.

3.1.2. Disc-shaped structure (h = 0.36–0.82 mm)

Continue to increase the liquid layer thickness, the spotted cavitation bubble clusters interact and connect with each other, and form large areas of uniformly distributed cavitation bubble clusters and disc-shaped structure (with curved boundary). For more detailed information about disc-shaped cavitation structure see also [17].

3.1.3. Rod-shaped structure (h = 1.23–3.24 mm)

Continue to increase the liquid layer thickness, the diameter of disc-shaped structure will increase, and the area of uniformly distributed cavitation cluster will be smaller until it becomes a rod-shaped structure. The main subject of this research is the rod-shaped structure. Within this range, the smoker structure will often appear.

3.1.4. Smoker structure (h > 4.54 mm)

Continue to increase the liquid layer thickness, the rod-shaped cross links become more and more sparse until it disappears. Only smoker structure exists in the thin liquid layer. In fact, in this range, the cavitation cloud cannot fill the gap (touch both radiating surface and reflecting surface), some smoker structure attached on the radiating surface, some smoker structure attached on the reflecting surface. For more detailed information about smoker cavitation structure see also [11].

It is found in the experiments that although the shape of cavitation cloud is complicated and variable, there are some stable feature element (the specific shape of the boundary between the cavitation cloud region and the non-cavitation liquid region) in cavitation structure. Spotted structure, disc-shaped structure, rod-shaped structure and

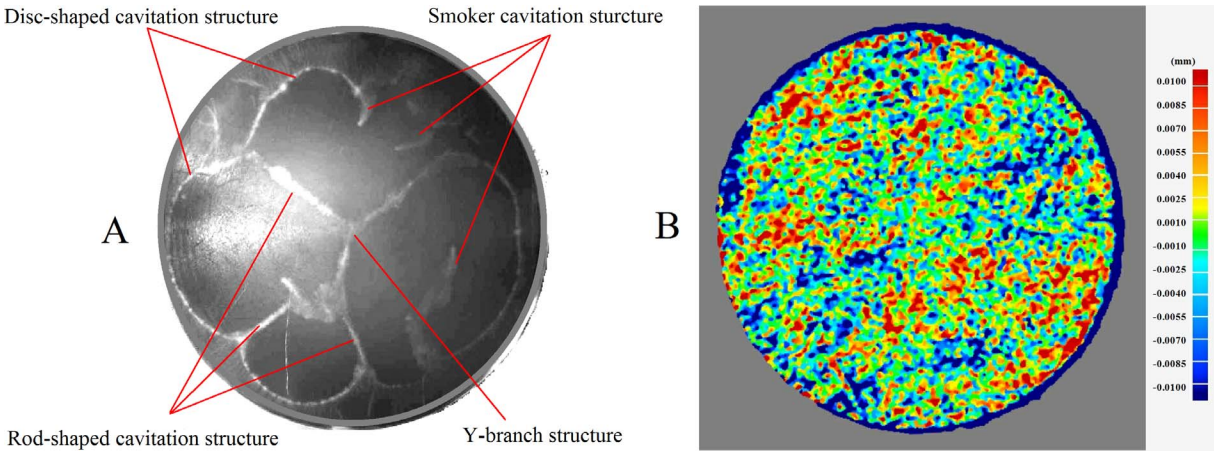

Fig. 3. Radiating surface of transducer (f = 20 kHz, d = 50 mm) (A). Feature elements of cavitation structure in the thin liquid layer (h = 1.23 mm); (B) The surface height difference distribution of the transducer, measured by Laser ranging techniques.

smoker structure can be considered as the feature elements of cavitation bubble distribution in thin liquid layers. A certain kind of stable feature element may be dominant in a cavitation structure. However, there is a very long transition region between the two cavitation structures, and there is no clear dividing line. In addition, the transition state between two cavitation structures is unstable and there is no obvious feature element. A cavitation cloud is a combination of one or more feature elements (as shown in Fig. 3(A)). It needs to be pointed out here that the cavitation structure has nothing to do with the distribution of the roughness of the transducer surface in the experiments. In other words, the roughness distribution of the transducer surface is not the determining factor of cavitation structure (as shown in Fig. 3(B)).

3.2. Formation and characteristics of rod-shaped structures

The rod-shaped structure is characterized by a cavitation cloud in the shape of a rod. Both ends of the rod are connected to other rods or large areas of cavitation clouds. The rod-shaped structure can be produced by different processes.

Fig. 4 shows the interaction of two disc-shaped structures. The two disc-shaped structures move towards each other, and the cavitation cloud between them becomes smaller and thinner. When a level is reached, the cavitation cloud between the two disc-shaped structures no longer decreases, and the width remains stable over time. A rod-shaped structure is formed in this way. This process is similar to the process of two soap bubbles coming close to each other. The collision of disc-shaped structures often occur during the random movement of cavitation cloud (as shown in Fig. 4), when varying the layer thickness from thin to thick (as shown in Fig. 2), or when the artificially implanted cavitation nuclei dissipate in large quantities.

Fig. 5 shows the process of formation of rod-shaped structure caused by the connection of two smoker structures. At first, the two smoker structures approach each other. When the heads of smokers are very close, they repel each other. With the accumulation of cavitation bubbles in the head of smokers, two smoker structures connect to each other, and a rod-shaped structure is formed. In fact, it is not common for two smoker heads to be directly linked to a rod-shaped structure. The large bubbles (or dense plume structures) in the middle part of the two separate smoker structures tend to attract each other driven by the secondary Bjerknes force. It was found that large bubbles or bubble clusters tend to deviate from the direction of primary Bjerknes forces and move towards each other, even when they are far away from each other. The secondary Bjerknes force is responsible for the interattraction of large bubbles or bubble clusters [10]. As a result, the two smoker structures bend towards each other and merge. A rod-shaped structure is more likely to form in this way with the original smoker structure (one or both) still “alive”. The bubbles or bubble clusters in the smoker structure move from the head to tail (as shown in Fig. 5(B)), while the bubbles or bubble clusters in the rod-shaped structure stay in the original place or move towards a larger cavitation cluster (as shown in Fig. 5(C)). Connection of smoker structures often occurs during the random movement of cavitation cloud (as shown in Fig. 2(A7–A9)).

Similar to the smoker structure, the rod-shaped structure is also composed of a few large bubbles and numerous small bubbles. The large bubbles which are attached to the radiating surface and surrounded by a large number of small bubbles align themselves along the

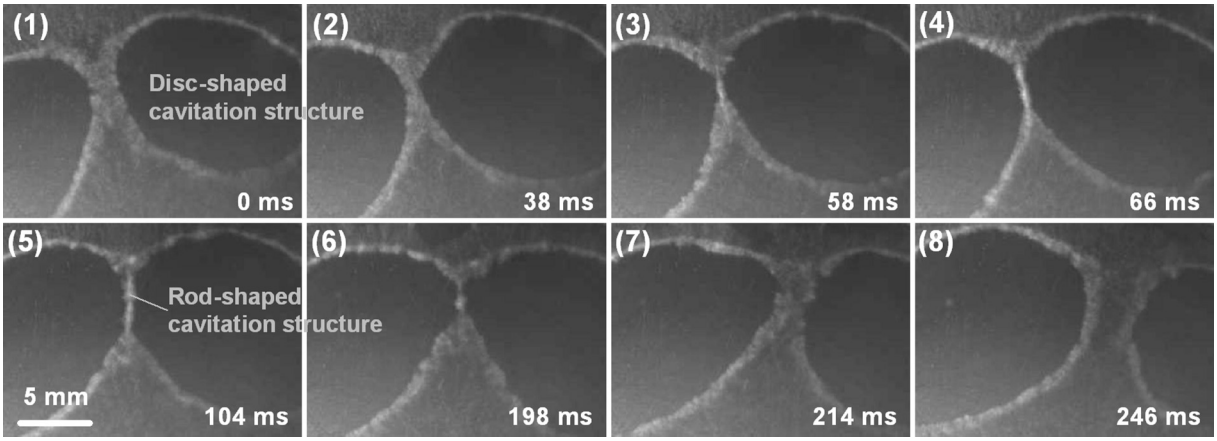

Fig. 4. Formation of rod-shaped structure caused by the collision of two disc-shaped structures.

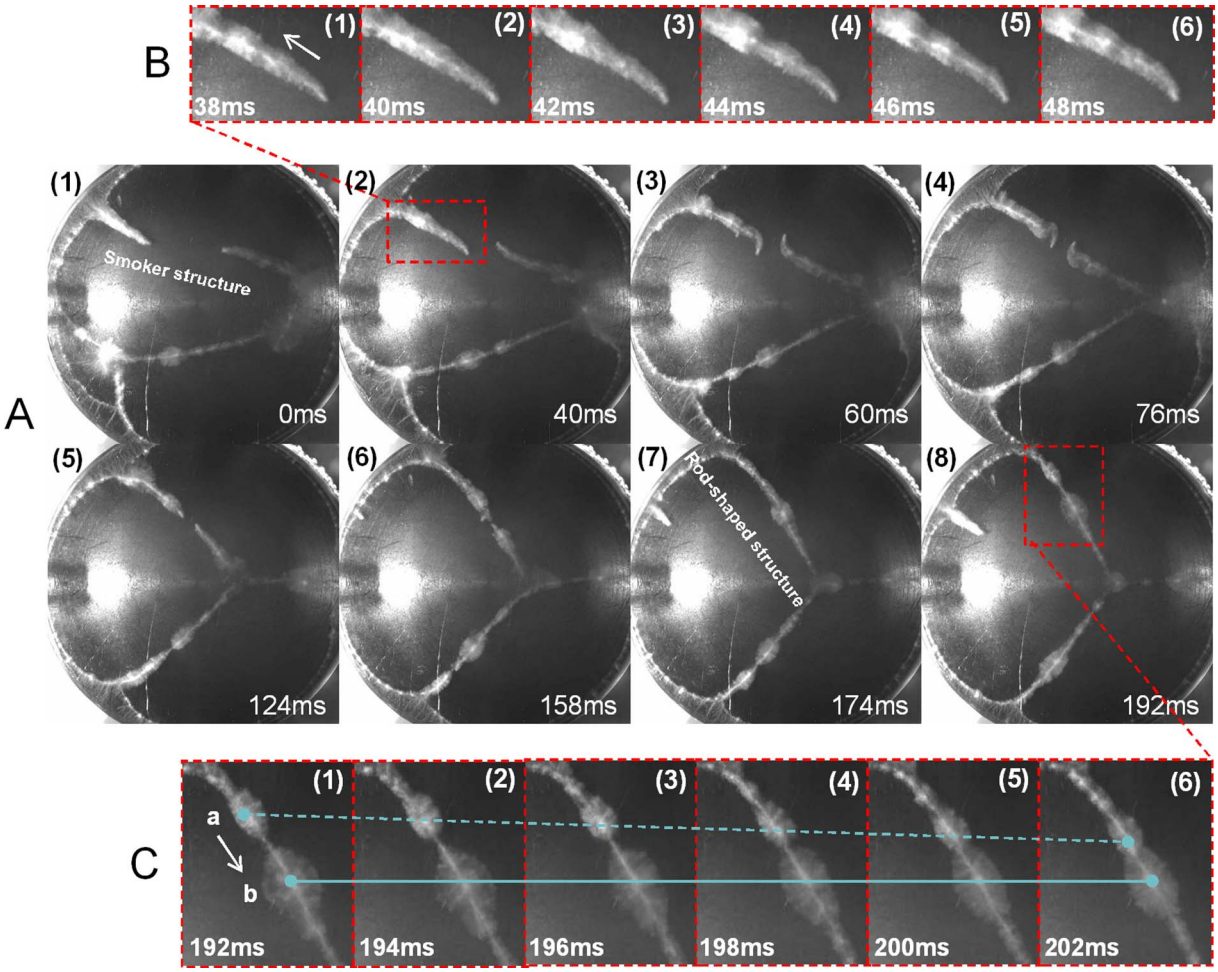

Fig. 5. Formation of rod-shaped structure caused by the connection of two smoker structures (Exposure time 1/500 s). (A) The interaction of two smoker structure. (B) The motion of bubble cluster in the smoker structure. (C) The motion of bubble cluster in the rod-shaped structure.

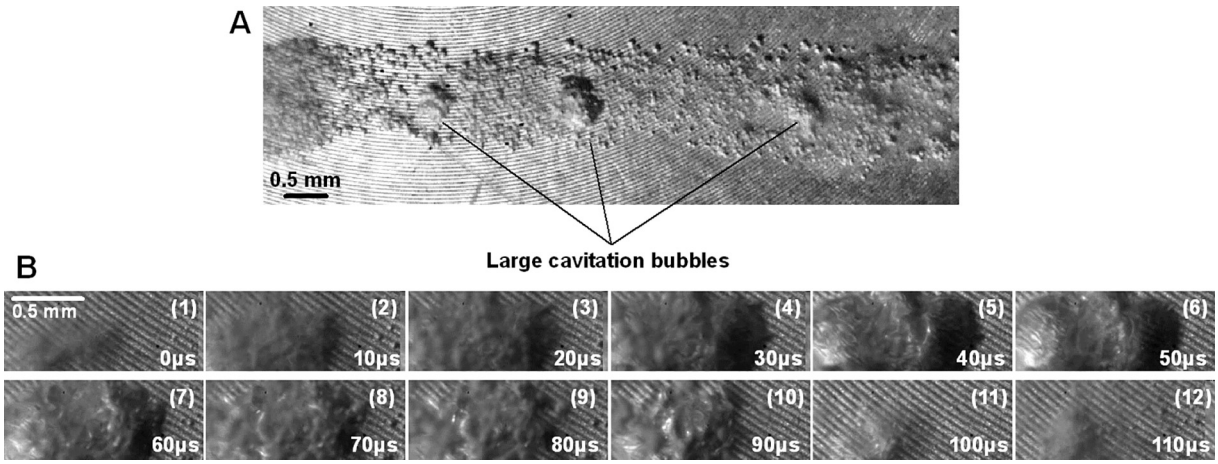

Fig. 6. Large cavitation bubbles in rod-shaped structures. (A) A rod-shaped structure with large bubbles aligns themselves along the central line (Exposure time 1/92,000 s). (B) The growth and collapse of a large cavitation bubble (Exposure time 1/100,000 s).

central line (as shown in Fig. 6(A)). A large bubble may exist as an individual bubble in one cycle, and may exist as a small bubble group in next cycle. The high-speed photos show that the approximate hemispherical surface of the bubble is very irregular in its maximum volume, and retains the characteristics of multiple bubbles merging (as shown in Fig. 6(B)).

In the high-speed photograph of long exposure time, the rod-shaped structure presents a clear central axis (as shown in Fig. 5). The presence of the central axis is partly because at some point larger bubbles (surrounded by a large number of small bubbles) lie in the axis of the rod-shaped structure (as shown in Fig. 6). Another important reason is the visual effect of image superposition caused by long exposure time (as shown in Fig. 7). The cavitation bubbles in the rod-shaped structure will not collapse at the same time. The small bubbles at the periphery will collapse first (the large bubbles may still be expanding when small bubbles collapse.), and then the large bubbles at the central line

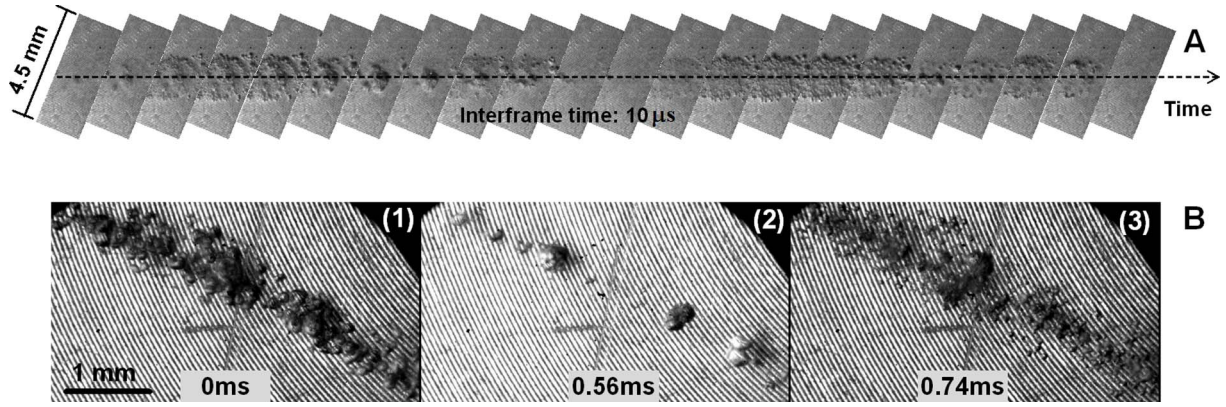

Fig. 7. The formation of central axis of rod-shaped structures. (A) The growth and collapse of a section of rod-shaped structure (Exposure time 1/119,000 s). (B) The snapshots of a rod-shaped structure (Exposure time 1/333,000 s).

collapse. A photograph of long exposure (for example, the exposure time is 1/500 s) is the overlay of images of the bubble cloud in 40 acoustic cycles. The central axis of rod-shaped structure is highlighted by this effect.

The width of rod-shaped structure is not absolutely uniform. In some places, it is wider than in others (as shown in Fig. 5(C)). The high-speed photograph shows that a cavitation bubble group with larger bubbles in the center is responsible for the enlargement of width (as shown in Fig. 8). It is an air enrichment zone, and there are even more bubbles and larger bubbles here than in other areas at each stage of acoustic cycles.

At larger magnification, it is found that unlike large cavitation bubbles, small cavitation bubbles are nearly perfect spherical (as shown in Fig. 9). Some bubbles are clear and some bubbles are blurry in Fig. 9, it is because the lens has a very small depth of field, bubbles that do not appear on the focal plane will be blurred. It is obvious that the bubbles are distributed in the thickness direction.

It can be seen from Fig. 10(A) that cavitation bubbles in the thin liquid layer do have a distribution in the thickness direction. Some bubbles are attached to the radiating surface, some bubbles are attached to the reflecting surface, and some bubbles are suspended between two boundaries. Large bubbles tend to attach to the boundary, and small bubbles suspending between two boundaries tend to move towards the boundary (or towards the large bubbles on the boundary). There is a clear boundary between the liquid region and the cloud region. Fig. 10(B) shows the boundary of a bubble cluster. The bubbles on the boundary show different morphology at different stages, and there is a slight fluctuation in the boundary line. Fig. 10(C) shows the growth and collapse of cavitation bubbles in the cluster between two boundaries. The bubble cluster grows up slowly, and then collapses rapidly.

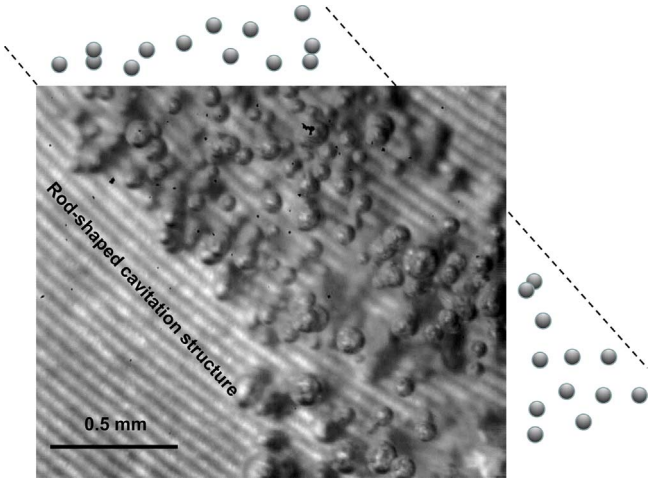

Fig. 9. A rod-shaped structure at high magnification (Exposure time 1/117,000 s).

Small bubbles in the cluster collapse first.

3.3. Y-branch structure in thin liquid layers

When many rod-shaped cavitation structures appear in the thin liquid layer, the rod-shaped structures will crosslink with each other to form a network distribution. The crosslinking is not random, and the rod-shaped structures will form Y-branch structures (as shown in Figs. 11, 2(A8), 3(A) and 5(A8)).

As a result of the motion (evolution) of cavitation structures, four rod-shaped structures may converge at one point in very rare cases (as

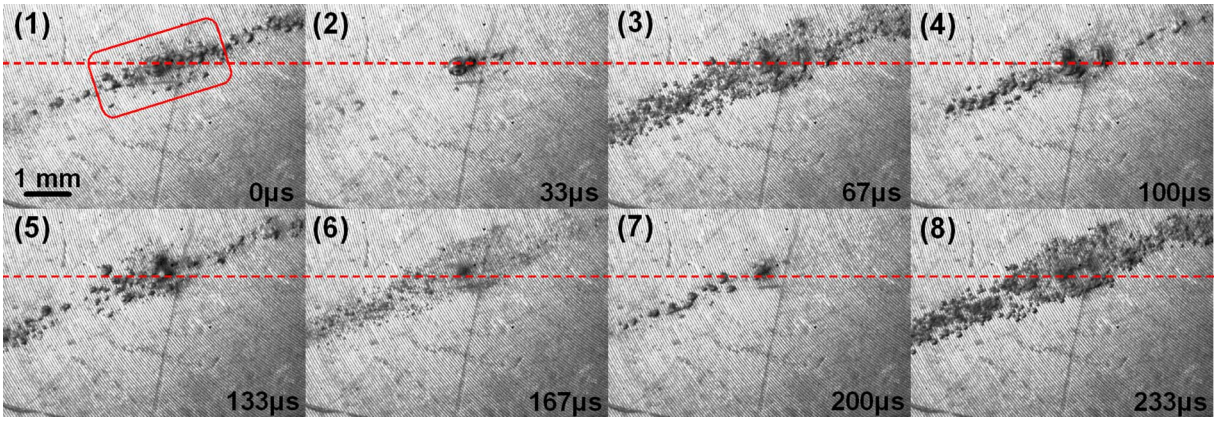

Fig. 8. A cavitation bubble group in the rod-shaped structure (Exposure time 1/551,000 s).

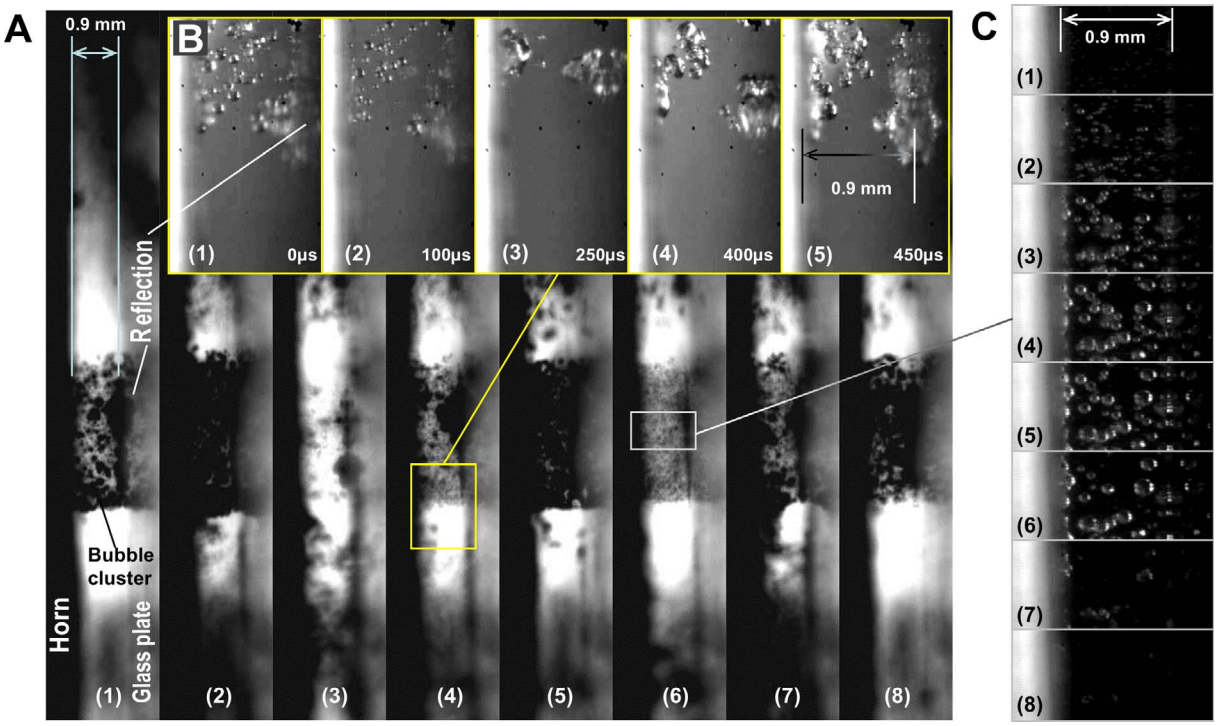

Fig. 10. The cavitation bubble cluster in a thin liquid layer (side view). (A) The growth and collapse of a cavitation bubble cluster. (Framing rate 5400 fps; Exposure time 1/74000 s.) (B) The boundary of a bubble cluster. (Exposure time 1/307000 s.) (C) The cavitation bubbles in a cluster. (Framing rate 125,000 fps; Exposure time 1/298,000 s.)

shown in Fig. 12(A)). The four-rod structure is unstable; it will be split into two Y-branch structures almost immediately after it is formed. The Y-branch structure is very stable; it can exist stably for a long time. This property is similar to that of soap bubbles (as shown in Fig. 12(B)). Due to the rupture of one of the soap bubbles, the foam will appear as a four-fold structure in the process of rebalancing. But this structure is very unstable, and it will soon evolve into two stable trigeminal structures (plateau border). In the next section, we will analyze the stability of the Y-branch structures.

It is found that although the position and shape of the cavitation cloud change greatly with time, the Y-branch structures are very stable. We monitored the angles of a rotating Y-branch structure within 1.2 s, and found that the three angles of the Y-branch structure remained at about 120 degrees (as shown in Fig. 13). The movement of intersection point of the Y-branch structure is shown in the upper right corner of Fig. 13. The time interval between adjacent points is 0.02 s. It can be seen that the change in position, the velocity of motion and the direction of motion of intersection point does not affect the angles of the Y-branch structure. The movement of the intersection point is caused by the constant change of the pressure field. A more detailed explanation is made in the next section.

To eliminate the specificity caused by the limited selection, we have made a statistical analysis of the Y-branch structures in a cavitation experiment lasting 3.9 s. A total of 54 Y-branch structures were sampled every 0.1 s, and 162 angles were measured. The statistics show that the probability distribution of the angle is a Gauss distribution

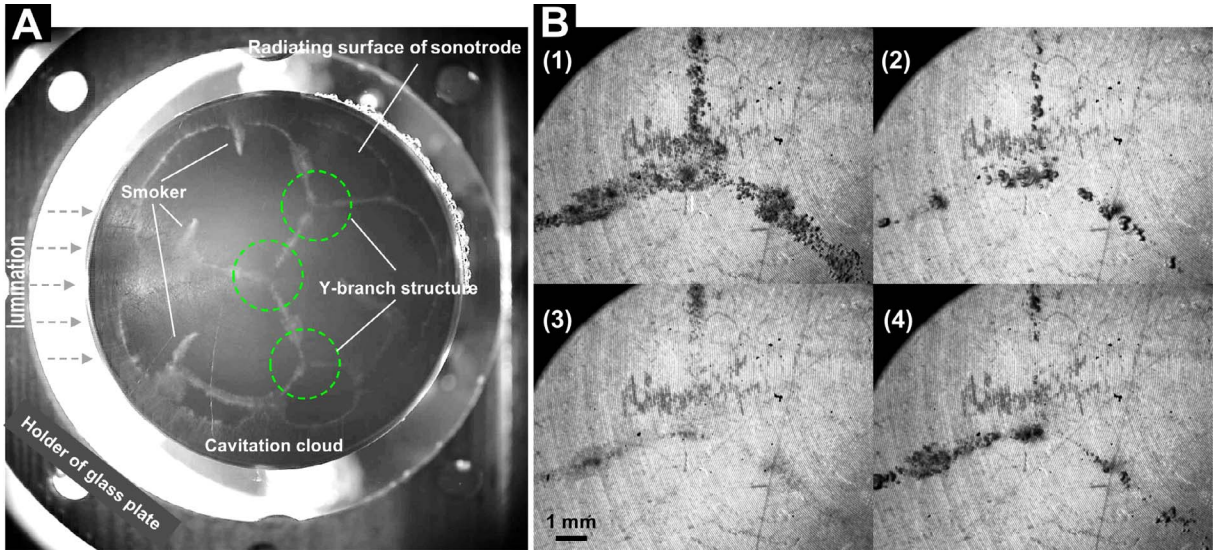

Fig. 11. Y-branch structures in a thin liquid layer. (A) Various cavitation structures on the radiating surface of sonotrode (Exposure time 1/500 s.) (B) A larger image of a Y-branch structure (Framing rate 5400 fps; Exposure time 1/593,000 s.)

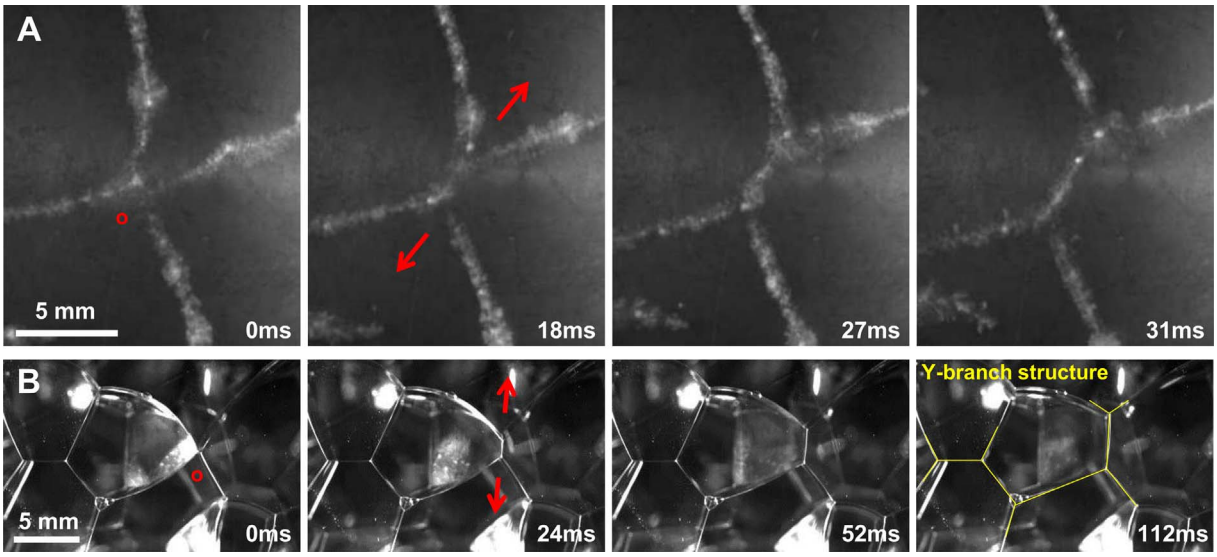

Fig. 12. Stability of Y-branch structures. (A) The four-rod cavitation structures intersecting at one point will be split into two Y-branch structures. (B) An analogy with soap bubbles.

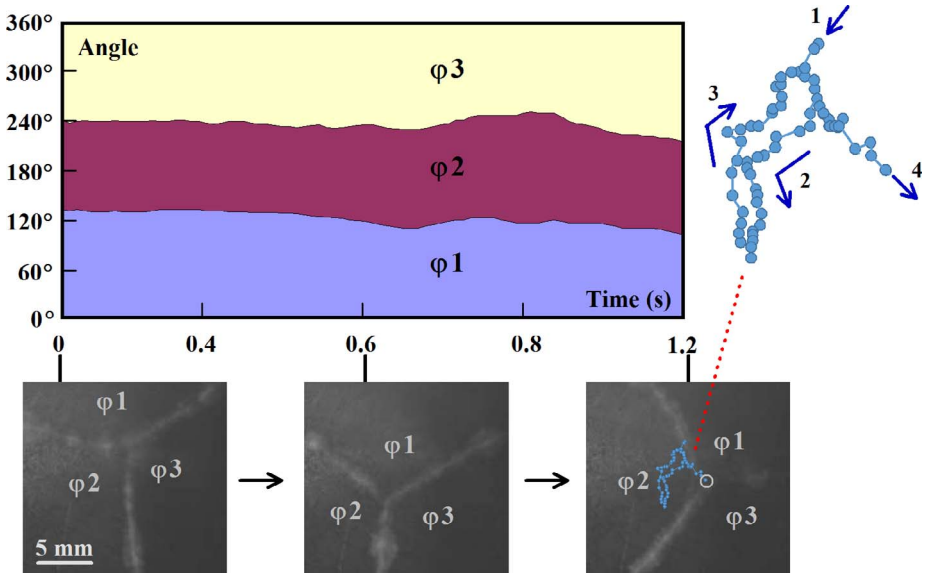

Fig. 13. The change of the angle of Y-branch structures with time.

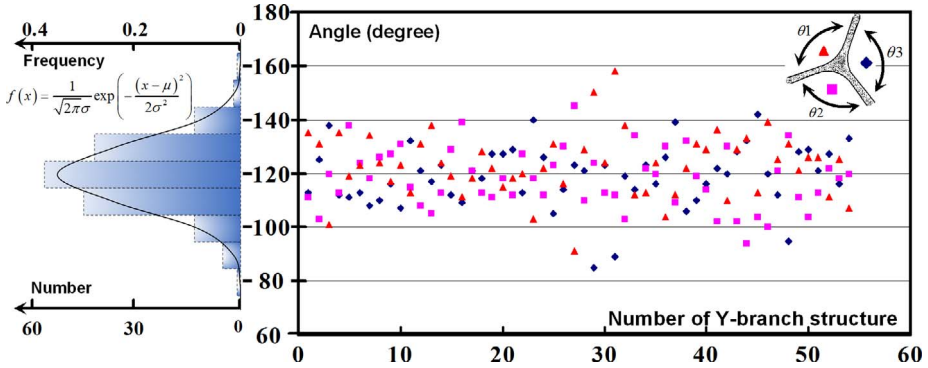

Fig. 14. The probability distribution of the angles of the Y-branch structures.

(mathematical expectation $\mu = 119.93$, standard deviation $\sigma = 11.64$) (as shown in Fig. 14). The three angles of every Y-branch structure tend to be equal (120 degrees), which is similar to the structure of soap bubbles.

Because the sound field distribution and the cavitation cloud distribution cannot form a long-term and stable mutual strengthening effect, the cavitation cloud formed by the Y-branch structures will continue to move (as shown in Fig. 15(A)). Relative to the speed of cavitation bubble collapse, the moving speed of rod-shaped structures is too small, and can be considered to be fixed (as shown in Fig. 15(B)).

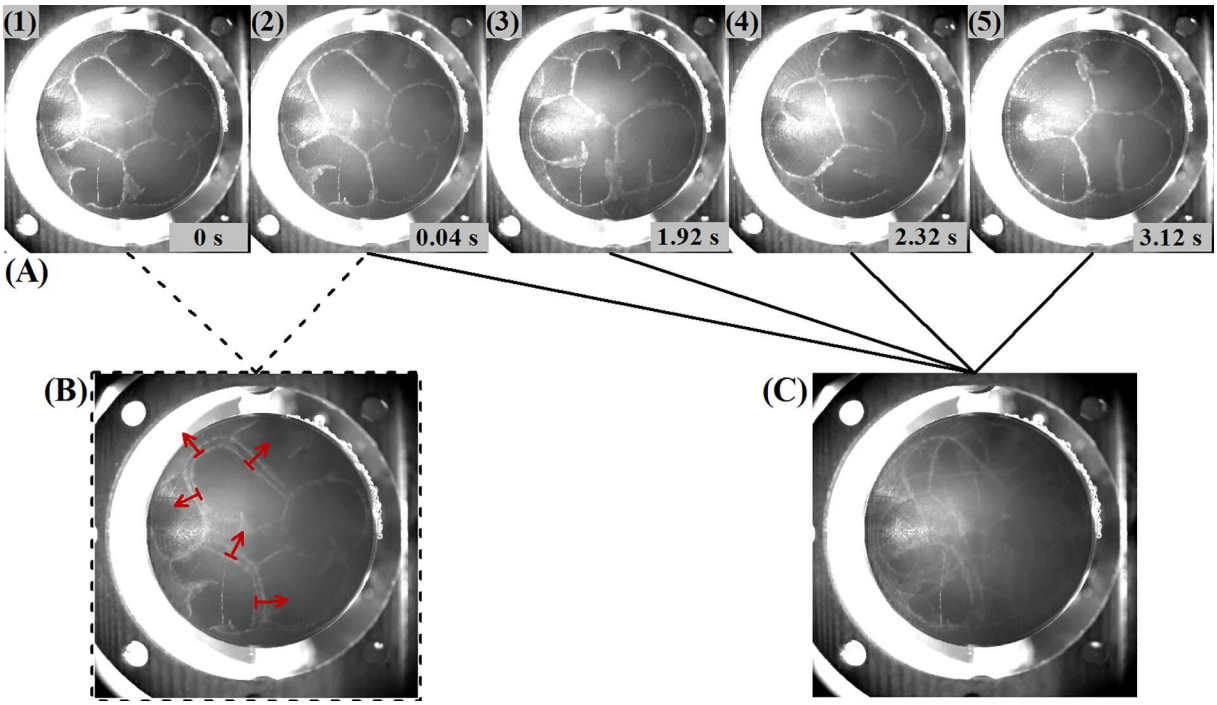

Fig. 15. The motion of Y-branch structures. (A) Cavitation structures at different moments. (B) A composite image of superimposing the first two high-speed photos. (C) A composite image of superimposing the last four high-speed photos.

Compared with the macroscopic migration velocity of the cavitation bubble, the moving speed of rod-shaped structures cannot be ignored. Although the cavitation cloud is unevenly distributed in space, it has a space-time ergodicity property (as shown in Fig. 15(C)).

3.4. The mechanism of formation of rod-shaped structure

The inhomogeneous distribution of cavitation clouds in a thin layer is partly caused by (and responsible for) the uneven distribution of sound field. The cavitation cloud and the sound field interact with each other, but they cannot reach the complete equilibrium, so the shape and position of the cavitation cloud will continue to evolve. Because the expected distribution of cavitation clouds is related to the distribution of cavitation nuclei, and the distribution of cavitation nuclei is related to the distribution of cavitation clouds of present, the cavitation clouds have obvious continuity. Due to the wall effect of the cavitation cloud restricting the lateral migration of the cavitation cloud, the motion of cavitation cloud shows hysteresis. Also due to the attraction of cavitation clouds caused by the secondary Bjerknes forces, cavitation clouds show a certain integrity. Since there is no cavitation bubble in the liquid region (non-cavitation region), the sound energy is not dissipated by the bubble cloud, so the sound pressure amplitude is higher. In contrast, the amplitude of sound pressure is lower in the cloud region (cavitation region) because of the absorption and scattering of the cavitation bubbles. The primary Bjerknes forces will cause cavitation bubbles to gather in the region of low pressure amplitude (cloud region), which tends to maintain the existing cavitation structure. Thus, in such a physical environment, in this section, we will analyze some feature elements of cavitation structures, such as smoker cavitation structure, rod-shaped cavitation structure, and the Y-branch cavitation structure (as shown in Fig. 16).

The shape of the smoker structure is similar to that of the rod-shaped structure, both of which are slender (as shown in Figs. 2(A10), 5(B) and 11(A)). The smoker cavitation structure can be considered as a special rod-shaped cavitation structure with source. We can divide a smoker structure into three parts. Part A is the head of smoker structure, which consists of some larger cavitation bubbles. The head of smoker structure contains more gas, even when the cavitation bubbles in other parts of smoker collapse, there are still some large bubbles in the head of smoker that did not collapse (as shown in Fig. 17(A1, A3)). The gas bearing behavior of head makes it the source of the cavitation nuclei [21]. When the pressure amplitude in a region exceeds a threshold value, cavitation bubbles tend to move along the direction of pressure drop [8,17]. Because of the pressure gradient, the cavitation bubbles (which form the middle part (part B) of the smoker structure) produced by the nuclei source are pushed to the low pressure amplitude region (cloud region) by the primary Bjerknes forces. This causes the head of smoker to always point to the center of the liquid region (high pressure amplitude region). The primary Bjerknes force ($F_{Bjerknes}^{primary}$) and the surface tension of bubble cloud ($F_{surface}$) tend to push the large cavitation bubbles in the head toward the tail of the smoker structure, but these bubbles usually stay where they are. This is because these bubbles are subjected to an opposite force (F_{pit}). The head of smoker structure is located in region of high pressure amplitude, so the bubbles in the head collapse violently. These bubbles will attach to the wall surface due to the strong secondary Bjerknes forces (Acoustically hard object surfaces can attract bubbles due to reflections (mirror effect)). The motion of these bubbles will be blocked by the micro-pit on the wall, resulting in an adhesion force (F_{pit}). It is found in the experiment that almost all the bubbles in the head of smoker structures are attached to the wall, which is consistent with the analysis. The bubbles in the head may merge together during the expansion, but they do not form a single hemispherical large bubble. Instead they form a thin layer of gas with an uneven surface (as shown in Fig. 17(B)).

Part B is the middle part of the smoker structure. The width of this part of smoker is approximately equal, and it is straight rod-shaped. Because the radius of curvature is infinite, the surface tension of bubble cloud ($F_{surface}$) is equal to 0. Due to the pressure gradient, the primary Bjerknes force ($F_{Bjerknes}^{primary}$) causes the bubbles on both sides to converge to the axis. At the same time, the secondary Bjerknes forces ($F_{Bjerknes}^{secondary}$) between the bubbles also makes the cluster converge, so the large bubbles which are attached to the radiating surface tend to align themselves along the central line, and numerous small bubbles move towards to the large bubbles. The forces are not balanced in the axial

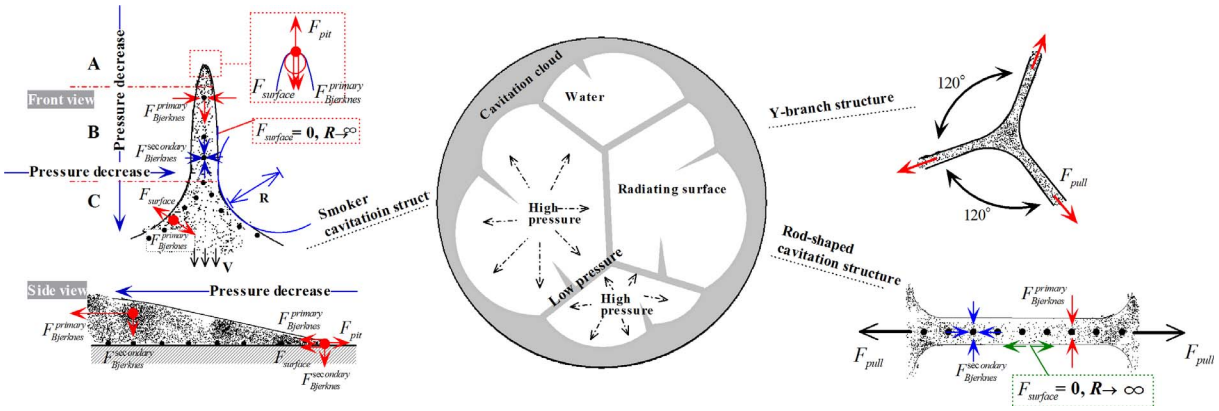

Fig. 16. Schematic diagram of the mechanism of formation of rod-shaped cavitation structure.

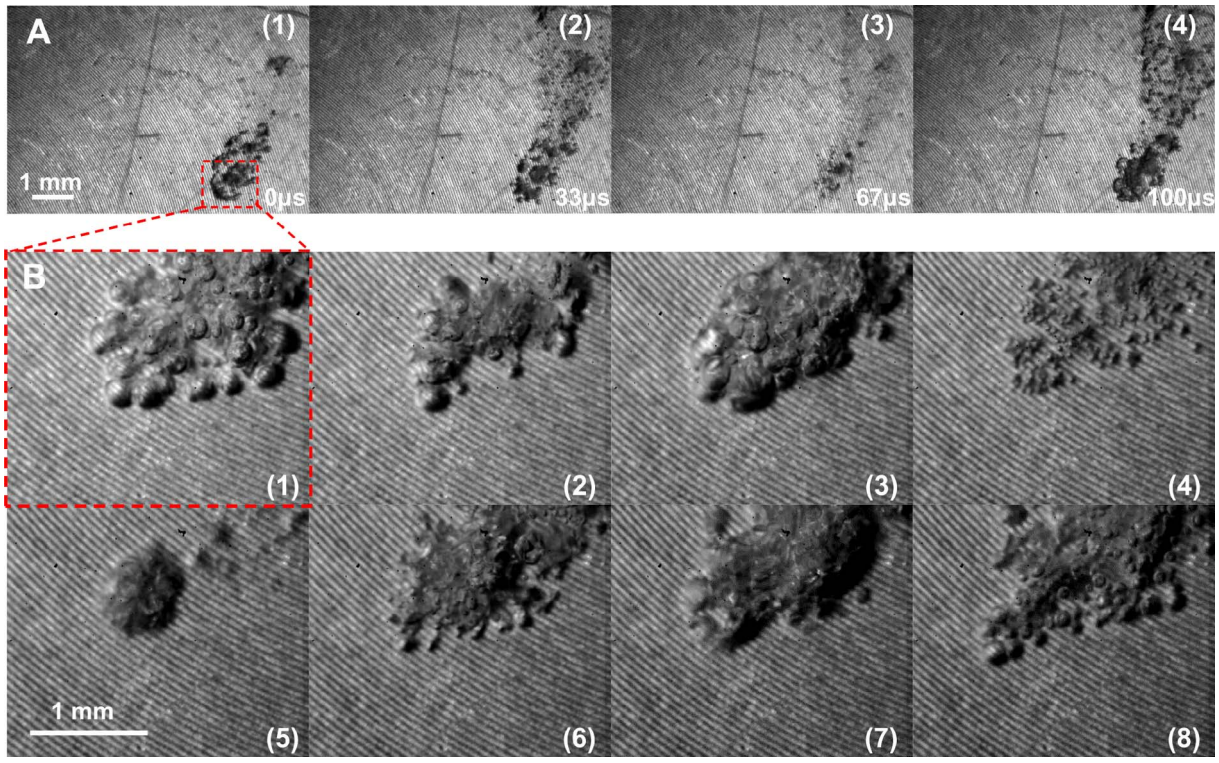

Fig. 17. Smoker structures on the radiating surface. (A) The growth and collapse of a smoker structure. (Exposure time 1/551,000 s.) (B) The growth and collapse of the head of a smoker structure. (Framing rate 12,000 fps; Exposure time 1/183,000 s.)

direction, and the bubbles move to the tail of smoker structure under the action of the primary Bjerknes force ($F^{primary}_{Bjerknes}$) (the secondary Bjerknes forces is balanced in the axial direction). The cavitation cloud gradually thickens as it moves toward the tail. Large bubbles and small bubbles attached to the wall move slower than the small upper ones due to the effect of the primary Bjerknes force ($F^{primary}_{Bjerknes}$) and the wall blocking effect. Part C is the tail of the smoker structure. The tail is widened and is often connected with a large area of cavitation clouds. Due to the effect of surface tension, the cavitation cloud at the tail has a circular-arc boundary on both sides [17]. The translational velocity of the cavitation bubbles at the center of the tail decreases gradually and is fused with a large area of cavitation cloud.

Both ends of the rod-shaped structure are connected to a large area of cavitation clouds or other rod-shaped structures. Due to the pressure gradient in the normal direction, the primary Bjerknes force ($F^{primary}_{Bjerknes}$) causes the bubbles on both sides to converge to the axis. At the same time, the secondary Bjerknes forces ($F^{\sec ondary}_{Bjerknes}$) between the bubbles also makes the cluster converge, so the large bubbles which are attached to the radiating surface tend to align themselves along the central line, and numerous small bubbles move towards to the large bubbles. There is no pressure gradient in the axial direction, so the bubbles will not move along the axis, but the large bubbles in the cavitation cloud may sometimes merge. Because the radius of curvature is infinite, the surface tension of bubble cloud in the normal direction ($F_{surface}$) is equal to 0. Because of the surface tension in the axis direction and the secondary Bjerknes forces ($F^{\sec ondary}_{Bjerknes}$) between the bubbles, the rod-shaped structure is subjected to a macroscopic tension in the axis direction (F_{pull}). The rod-shaped structure has contact with the both upper and lower walls, so there is no difference in thickness.

Most of the rod-shaped structures in the thin liquid layer can be approximately regarded as straight rods, but careful measurements show that many rod-shaped structures have certain curvature (as shown in Fig. 18). The Y-branch structure in Fig. 18 consists of rod A, rod B, and rod C. In the evolution of cavitation clouds, the intersection point O moves to the upper right. The rod C keeps straight, but the rod A and the rod B bend, and their curvature increases with time (as shown in

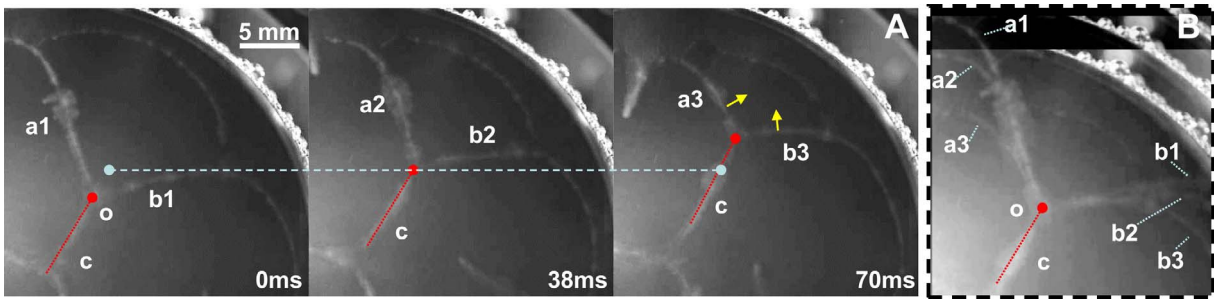

Fig. 18. Curved rod-shaped structure. (A) The evolution of a Y-branch structure. (B) A composite image of superimposing the high-speed photos in (A).

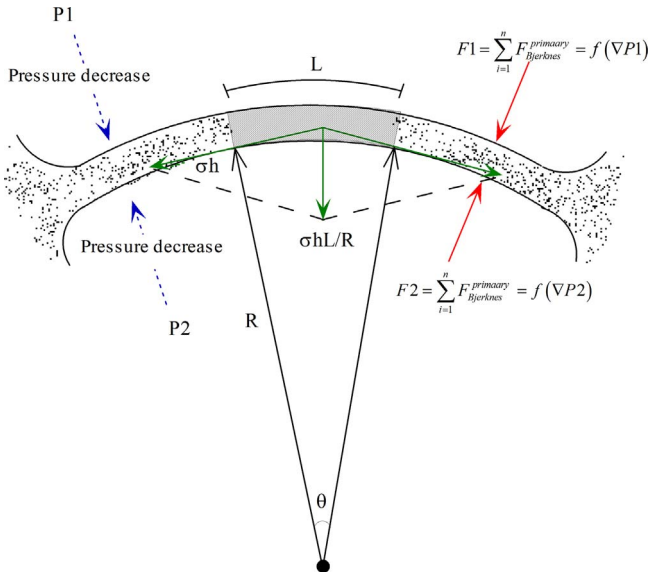

Fig. 19. Schematic diagram of the mechanism of formation of curved rod-shaped structure.

Fig. 18(B)). It is found that the liquid region AOC and BOC is close to the high pressure amplitude region (the center of the transducer), and their areas become larger with time; while the liquid region AOB is close to the low pressure amplitude region (the edge of the transducer), and its area becomes smaller with time. The bending of rod-shaped structure is related to the force exerted (Fig. 19).

In the time scale of the bubble pulsation, the macroscopic motion of the cavitation cloud can be neglected. We believe that the time evolution of the cavitation cloud is a quasi-static process, that is, the forces exerted on the cavitation cloud is balanced all the time. By regarding the bubble cloud as a whole, it is possible to make a mechanical analysis on the curved rod-shaped structure with a radius of curvature of R. Both sides of the curved rod-shaped structure are high pressure amplitude region (liquid area), the pressure is *P1* and *P2* respectively, while the cavitation cloud is in the low pressure amplitude region. Due to the pressure gradient, the bubbles in the cavitation cloud is governed by the primary Bjerknes force ($F_{Bjerknes}^{primary}$). If we define the macroscopic force along the normal direction due to the pressure gradient $\nabla P1$ acting on the unit length is $F1=\sum_{i=1}^{n}F_{Bjerknes}^{primary}=f(\nabla P1)$, the macroscopic force along the normal direction due to the pressure gradient $\nabla P2$ acting on the unit length is $F2=\sum_{i=1}^{n}F_{Bjerknes}^{primary}=f(\nabla P2)$, the resultant force (in normal direction) which exerted on the curved rod-shaped structure with length of L is $(F2-F1)\,L$. We define the surface tension of the cavitation cloud (σ) as the pulling force between the cavitation clouds of unit length along the tangent plane of the radiation surface, so the resultant force due to the surface tensions along the normal direction of the curved rod-shaped structure with length of L is $2\sigma h\sin\left(\theta/2\right)$ (h is the thickness of the thin liquid layer). When θ approaches 0, $\sin(\theta)$ is approximately equal to θ, $2\sigma h\sin\left(\theta/2\right)\approx \sigma hL/R$. Force balance in normal direction:

$$F2-F1=2\sigma h/R$$

In Fig. 18, the difference between the macroscopic forces of rod A and rod B in the normal direction becomes larger with time. In order to keep the equilibrium state, according to the above formula, the curvature will inevitably become larger with time. These properties are similar to those of soap bubbles.

The bubbles at the intersection of Y-branch structure are shared by the three rod-shaped structures, they interact with each other, and the motion of the bubbles in each rod-shaped structure has no fixed direction, so the intersection point is easy to move. The Y-branch structure can be regarded as a hinge structure without any restraint, which can slide on any of the rod-shaped structures. This structure is the same as the equilibrium structure formed by three equal non-directional forces in space, which is not uncommon in nature. Plateau boundary of soap bubbles is an example of this structure, according to the Plateau law [22], the structure of three rods is the most stable, and the angle between the rods is 120 degrees. This is consistent with the experimental results mentioned above.

4. Summary and conclusions

Rod-shaped cavitation bubble structures in thin liquid layers in ultrasonic field are investigated experimentally. It is found that the cavitation structure successively experiences several stages with the change of the thickness of the thin liquid layer, such as spotted structure, disc-shaped structure, rod-shaped structure, and smoker structure. A Rod-shaped structure can be formed by the collision of two disc-shaped structures or by the connection of two smoker structures. Rod-shaped structure presents a clear central axis, which is partly because larger bubbles lie in the axis of the structure, and another important reason is the visual effect of image superposition caused by long exposure time. Cavitation bubbles in the thin liquid layer have a distribution in the thickness direction. Large bubbles tend to attach to the boundary, and small bubbles suspending between two boundaries tend to move towards the boundary (or towards the large bubbles on the boundary). The rod-shaped structures tend to crosslink with each other to form stable Y-branch structures. The statistics show that the probability distribution of the angle of the Y-branch structure is a Gauss distribution with mathematical expectation $\mu = 119.93$ and standard deviation $\sigma = 11.64$. The head of smoker structure consists of some larger cavitation bubbles (contains more gas), which makes it the source of the cavitation nuclei. Because of the pressure gradient, the cavitation bubbles produced by the nuclei source are pushed to the low pressure amplitude region by the primary Bjerknes forces, which causes the head of smoker to always point to the center of the liquid region. The motion of these bubbles in the head will be blocked by the micro-pit on the wall, resulting in an adhesion force opposite to the primary Bjerknes force and the surface tension of bubble cloud. Due to the

pressure gradient in the normal direction, the primary Bjerknes force causes the bubbles in the rod-shaped structure on both sides to converge to the axis. The secondary Bjerknes forces between the bubbles also make the cluster converge, so the large bubbles which are attached to the radiating surface tend to align themselves along the central line. According to the formula deduced in this paper, the variation of curvature of curved rod-shaped structure is qualitatively analyzed. There are some similarities between the Y-branch structure of cavitation cloud and Plateau boundary of soap bubbles.

Acknowledgments

This work was supported by the National Natural Science Foundation of China (No. 11674350, No. 51435004, No. 51572271), National Basic Research Program of China (973 Program) (No. 2016YFA0201500).

References

[1] L. Bai, W. Xu, Z. Tian, N. Li, A high-speed photographic study of ultrasonic cavitation near rigid boundary, J. Hydrodyn. Ser. B 20 (2008) 637–644.
[2] R. Mettin, Bubble structures in acoustic cavitation, in: A.A. Doinikov (Ed.), Bubble and Particle Dynamics in Acoustic Fields: Modern Trends and Applications, Research Signpost, Kerala, 2005, pp. 1–36.
[3] A. Moussatov, C. Granger, B. Dubus, Cone-like bubble formation in ultrasonic cavitation field, Ultrason. Sonochem. 10 (2003) 191–195.
[4] B. Dubus, C. Vanhille, C. Campos-Pozuelo, C. Granger, On the physical origin of conical bubble structure under an ultrasonic horn, Ultrason. Sonochem. 17 (2010) 810–818.
[5] O. Louisnard, A simple model of ultrasound propagation in a cavitating liquid. Part II: primary Bjerknes force and bubble structures, Ultrason. Sonochem. 19 (2012) 66–76.
[6] L. Bai, W. Xu, J. Deng, C. Li, D. Xu, Y. Gao, Generation and control of acoustic cavitation structure, Ultrason. Sonochem. 21 (2014) 1696–1706.
[7] I. Akhatov, U. Parlitz, W. Lauterborn, Towards a theory of self-organization phenomena in bubble-liquid mixtures, Phys. Rev. E 54 (1996) 4990–5003.
[8] U. Parlitz, R. Mettin, S. Luther, I. Akhativ, M. Voss, W. Lauterborn, Spatio-temporal dynamics of acoustic cavitation bubble clouds, Philos. Trans. R. Soc. Lond. A 357 (1999) 313–334.
[9] R. Mettin, S. Luther, C.-D. Ohl, W. Lauterborn, Acoustic cavitation structures and simulations by a particle model, Ultrason. Sonochem. 6 (1999) 25–29.
[10] L. Bai, J. Deng, C. Li, D. Xu, W. Xu, Acoustic cavitation structures produced by artificial implants of nuclei, Ultrason. Sonochem. 21 (2014) 121–128.
[11] L. Bai, C. Ying, C. Li, J. Deng, The structures and evolution of Smoker in an ultrasonic field, Ultrason. Sonochem. 19 (2012) 762–766.
[12] R. Mettin, P. Koch, D. Krefting, W. Lauterborn, Advanced observation and modeling of an acoustic cavitation structure, in: O.V. Rudenko, O.A. Sapozhnikov (Eds.), Nonlinear Acoustics at the Beginning of the 21st Century, (Proceedings of the 16th International Symposium on Nonlinear Acoustics ISNA-16), vol. 2, Faculty of Physics, MSU, Moscow, 2002, pp. 1003–1006.
[13] D. Krefting, R. Mettin, W. Lauterborn, High-speed observation of acoustic cavitation erosion in multibubble systems, Ultrason. Sonochem. 11 (2004) 119–123.
[14] A. Moussatov, C. Granger, B. Dubus, Ultrasonic cavitation in thin liquid layers, Ultrason. Sonochem. 12 (2005) 415–422.
[15] G. García-Atance Fatjó, A. Torres Pérez, M. Hadfield, Experimental study and analytical model of the cavitation ring region with small diameter ultrasonic horn, Ultrason. Sonochem. 18 (2011) 73–79.
[16] L. Bai, W. Lin, P. Wu, J. Deng, C. Li, D. Xu, D. Wang, L. Chen, Memory effect and redistribution of cavitation nuclei in a thin liquid layer, Ultrason. Sonochem. 32 (2016) 213–217.
[17] L. Bai, X. Chen, G. Zhu, W. Xu, W. Lin, P. Wu, C. Li, D. Xu, J. Yan, Surface tension and quasi-emulsion of cavitation bubble cloud, Ultrason. Sonochem. 35 (2017) 405–414.
[18] P. Wu, L. Bai, W. Lin, J. Yan, Stability of cavitation structures in ultrasonic field, Ultrason. Sonochem. 38 (2017) 75–83.
[19] D. Fernandez Rivas, L. Stricker, A.G. Zijlstra, H.J.G.E. Gardeniers, D. Lohse, A. Prosperetti, Ultrasound artificially nucleated bubbles and their sonochemical radical production, Ultrason. Sonochem. 20 (2013) 510–524.
[20] A.G. Zijlstra, D. Fernandez Rivas, J.G.E. Gardeniers, M. Versluis, D. Lohse, Enhancing acoustic cavitation using artificial crevice bubbles, Ultrasonics 56 (2015) 512–523.
[21] L. Bai, W. Xu, C. Li, Y. Gao, The counter jet formation in an air bubble induced by the impact, J. Hydrodyn. Ser. B 23 (2011) 562–569.
[22] P. Ball, Nature's Patterns: A Tapestry in Three Parts, Oxford University Press, UK, 2009.